Engineering of Science and Military Technologies
Volume (1) - Issue (1) - 2017

ISSN: 2357- 0954
DOI: 10.21608/ejmtc.2017.449.1014

Non-linear skid steering system for 4×4 UGV using fuzzy logic direct yaw moment control

Original Article

Alhossein M. Sharaf

Automotive Engineering Department, Military Technical College, Cairo, Egypt

Key words:

Direct yaw moment, fuzzy logic control, skid steering system, unmanned ground vehicles.

Corresponding Author: Alhossein Mostafa Sharaf, PhD., Automotive Engineering Department, Military Technical College, Cairo, Egypt.
E-mail : a.m.sharaf@mtc.edu.eg

Abstract

This paper presents a non-linear control system for skid-steered 4×4 Unmanned Ground Vehicles (UGV) with an accurate representation of non-linear tire forces. The vehicle body dynamics is represented by three degrees of freedom (DOF) namely; forward, lateral and yaw movements. Additionally two DOFs are included to represent the angular rotations of both left and right wheels which are rigidly driven by a separate electric motor for each side. The proposed skid steering system is aimed to control both the driving speed and directional movement of the UGV body in order to follow a desired cornering scenario. Based on direct yaw moment control (DYC) method, a non-linear fuzzy logic controller is designed to regulate both the magnitude and direction of the output torque form each motor in-order to minimize the error between the desired and actual values of both yaw rate and side slip angle of the vehicle body. Several numerical simulations are carried out in MATLAB / Simulink environment to examine the fidelity of the proposed control system. Simulation results show the appropriateness of the proposed skid steering control system for the implementation in UGVs to perform prescribed cornering scenarios.

1. Introduction

Skid steering systems have been originally adopted for the military tracked vehicles where turning the vehicle is achieved by altering the driving torque or tangential speed across its left and right tracks. Furthermore, skid steering systems have been widely employed in multi-wheeled armored personnel carriers (APCs), load handling wheeled vehicles and robotic vehicles [1]. In comparison to Ackermann-steered vehicles, the skid steering systems offered many advantages such as significant increase in the internal hull volume and reduced turning radius during low speed tight cornering maneuvers. On the other hand, greater power and torque are required to generate higher differential tractive forces between left and right wheels which in turn increase the pneumatic tire wear, fuel consumption and reduced mileage range particularly on rigid roads and at higher cornering speeds [2].

Recently, the rapid development in automotive electric-driven systems including individual in-wheel motors has offered the possibility to design more efficient skid-steered controlled systems. The maneuverability of such vehicles is limited by the maximum allowable wheel differential torque which in turn depends on the available road adhesion and tires vertical weight. Further increase in the applied wheel differential torque causes more tire slip and reduces vehicle cornering stability [3]. Consequently, accurate calculations of tire forces and its associated slip is a milestone for the design of skid-steered control systems in wheeled ground vehicles.

For wheeled mobile robots and small electric vehicles, the basic modelling and control algorithms of skid steering systems have been broadly investigated, e.g. [4-7]. Normally, two separate electric motors are employed to drive both left and right wheels independently. Based on the desired speed and path, motion control is achieved by individually controlling the motors output torque and the wheels angular speed accordingly. The majority of the published work is based on simplified kinematical models which simply correlate the wheels angular velocities to the vehicle body linear velocity and the turning radius of the curvature. Furthermore, the tire forces are approximately calculated using linearized tire formulas which may be only suitable for path planning and motion control of indoor small car like robot. However, for full scaled UGVs with relatively higher weight which are performing typical field missions at moderate speeds, both body dynamics as well as tire forces should be sufficiently considered.

The concept of skid steering has been further extended to multi-wheeled light armored vehicles and military unmanned ground vehicles for the applications of pathfinder, surveillance and light combat operations, e.g. [8-12]. For such vehicle configurations, the drive-train is normally hybrid-electric or battery-electric powered with higher traction in-wheel motor at each wheel offering the advantages of optimized torque distribution, slip control and regenerative brake control.

However, to date, there is very little published research work which illustrate the dynamics of UGVs with skid steering system during transient and abrupt change maneuvers at relatively higher driving speeds.

In this paper, the proposed skid steering control system is based on direct yaw moment control (DYC) method in which yaw motion is generated due to the differential applied torque between the left and right wheels. The distributed torques of the individual electric motors are controlled to maintain the desired yaw rate and side-slip angle based on both the desired steering angle and vehicle driving speed.

The presented work starts with deriving the mathematical formulation of the unmanned ground vehicle, including body, drive-train, wheels and non-linear tire dynamics. Consequently, based on the direct yaw moment control (DYC) method, the design procedures of a skid-steered control system using fuzzy logic control are outlined. The results of UGV dynamic response during transient and abrupt lane change maneuver are then illustrated and analyzed.

2. Mathematical Formulation

This section outlines the mathematical model of a medium weight (1280 kg) all-terrain 4×4 unmanned ground vehicle. The vehicle body is rigidly connected to four driving wheels without suspension system and driven by two identical and separate high-performance permanent magnet synchronous electric motors (PMSM). For each side, the electric motor is rigidly connected to the rear wheel through a gear reduction unit and drives the front wheel at the same rotational speed using a chain.

The mathematical representation of the vehicle model is illustrated in Fig. 1 along with all moments and tire forces affecting the vehicle body dynamics. The UGV body is assumed to be rigid with a total mass concentrated at its center of gravity and has three degrees of freedom namely; forward translation in the longitudinal x-axis, lateral translation in the transverse y-axis and yaw rotation around the vertical z-axis. Based on Newton–Euler method, the equations of motion of the vehicle body for translational and rotational dynamics can be written as follows:

$$m\left(\dot{U}-V\cdot r\right)=F_{x_1}+F_{x_2}+F_{x_3}+F_{x_4}-0.5\rho C_d A_f U^2 \quad (1)$$

$$m\left(\dot{V}+U\cdot r\right)=F_{y_1}+F_{y_2}+F_{y_3}+F_{y_4} \quad (2)$$

$$I_{zz}\cdot\dot{r}=\left(F_{x_1}+F_{x_3}-F_{x_2}-F_{x_4}\right)c+\left(F_{y_1}+F_{y_2}\right)a-\left(F_{y_3}+F_{y_4}\right)b \quad (3)$$

Where $\left(F_{x_i}, F_{y_i}\right)$ are the generated tire forces in both longitudinal and lateral directions. (U,V,r) are the vehicle velocities in forward, lateral and around the vertical direction. According to the SAE recommended frame of reference, the vehicle dynamics is derived with respect to a vehicle-fixed frame of reference. Additionally, the vehicle trajectory is obtained relative to an earth-fixed frame of reference.

Considering Newton law for rotational dynamics, two differential equations are added to obtain the angular speed for both left and right wheels as follows, see Fig. 2.

$$J_{eq}\dot{\omega}_L=\xi M_{m_L}-\left(F_{x_1}+F_{x_3}\right)r_d-\left(F_{z_1}+F_{z_3}\right)t_p \quad (4)$$

$$J_{eq}\dot{\omega}_R=\xi M_{m_R}-\left(F_{x_2}+F_{x_4}\right)r_d-\left(F_{z_2}+F_{z_4}\right)t_p \quad (5)$$

It should be noted that, for each side, the front and rear wheels are constrained by a chain to rotate at the same angular speed $\left(\omega_1=\omega_3=\omega_L \text{ and } \omega_2=\omega_4=\omega_R\right)$ where the torque speed characteristics of the electric motor is shown in Fig. 3. The equivalent mass moment of inertia is: $J_{eq}=2J_w+J_m\xi^2$

Referring to (4) and (5), and assuming minor changes in dynamic tire vertical loads during cornering, it can be observed that, the angular wheel differential speed $\left(\omega_R-\omega_L\right)$ and therefore the lateral direction of the vehicle depends upon right and left wheel differential torque and the differential tire tractive forces as follow:

$$\omega_R-\omega_L=\frac{1}{J_{eq}}\int\left(\xi\left(M_{m_R}-M_{m_L}\right)+\left(F_{x_1}+F_{x_3}-F_{x_2}-F_{x_4}\right)r_d\right)\cdot dt \quad (6)$$

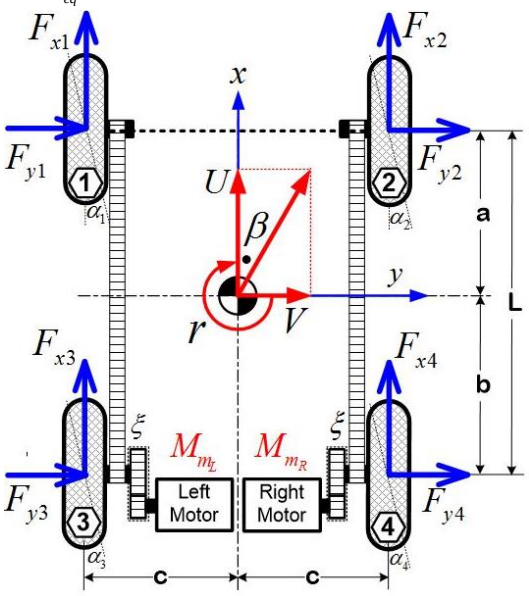

Fig. 1: Vehicle body forward, lateral and yaw dynamics

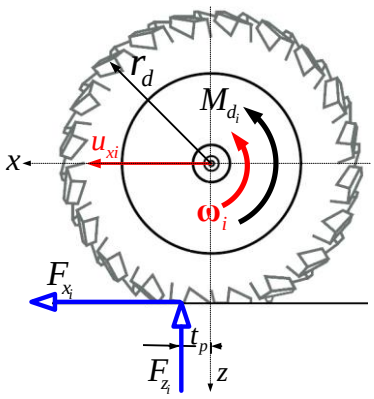

Fig. 2: Wheel rotational dynamics

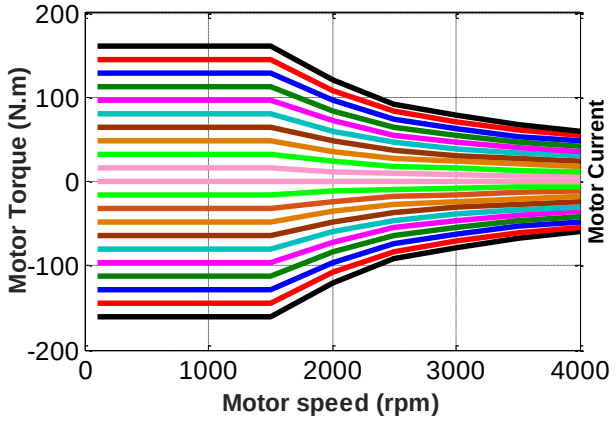

Fig. 3: Permanent magnet synchronous motors characteristics

It is widely known that, for a given value of tire vertical load (F_{z_i}) and road adhesion coefficient, the tire forces (F_{x_i}, F_{y_i}) are varying non-linearly with its longitudinal slip ratio (λ_i) and slip angle (α_i) respectively. Additionally, increasing tractive forces (F_{x_i}) will reduce the potential of tire lateral force (F_{y_i}) according to the concept of friction circle. Therefore, in this paper, the Magic Formula tire-model is employed to calculate tire forces as follow [13]:

$$y = D\sin\left[C\arctan\left(Bx - E\left(Bx - \arctan Bx\right)\right)\right] \qquad (7)$$

Where (y) represents the tire forces or moments, and (x) is the associated longitudinal slip, skid or cornering slip ratios. The magic formula's coefficients (B, C, D, E) are the stiffness, shape, peak and curvature factors respectively which are obtained based on measured data of tire forces and moments. From vehicle kinematics, both longitudinal slip ratio (λ_i) and slip angle (α_i) for each tire are calculated as follows:

$$\lambda_i = \frac{\omega_i \cdot r_d - u_{x_i}}{u_{x_i}} \quad and \quad \tan\alpha_i = -\frac{v_{y_i}}{u_{x_i}} \qquad (8)$$

Where (u_{x_i}, v_{y_i}) are the velocity components at the i[th] wheel center projected to the wheel orthogonal plane as follows:

$$\left.\begin{aligned} u_{x_1} &= U + cr \\ u_{x_2} &= U - cr \\ u_{x_3} &= U + cr \\ u_{x_4} &= U - cr \end{aligned}\right\} \quad and \quad \left\{\begin{aligned} v_{y_1} &= V + ar \\ v_{y_2} &= V + ar \\ v_{y_3} &= V - br \\ v_{y_4} &= V - br \end{aligned}\right. \qquad (9)$$

For each tire, the vertical force is calculated from the UGV static weight (mg) and the dynamic load due to forward and lateral accelerations (a_x, a_y) as follow:

$$\left.\begin{aligned} F_{z_1} &= \frac{b}{2L}mg - \frac{h}{2L}ma_x - \frac{bh}{2Lc}ma_y \\ F_{z_2} &= \frac{b}{2L}mg - \frac{h}{2L}ma_x + \frac{bh}{Lc}ma_y \\ F_{z_3} &= \frac{a}{2L}mg + \frac{h}{2L}ma_x + \frac{ah}{Lc}ma_y \\ F_{z_4} &= \frac{a}{2L}mg + \frac{h}{2L}ma_x - \frac{ah}{Lc}ma_y \end{aligned}\right\} \qquad (10)$$

3. Skid steering controller design

The structure of the proposed skid steering control system for 4×4 UGV is shown in Fig. 4. The driving torque from both left and right motors are controlled to follow a desired driving speed, steady state yaw rate and side slip angle. In the following sections, the main control blocks are explained.

3.1 Desired Yaw Rate and Side-slip Angle

In order to control the UGV direction and perform a desired or virtual steering angle (δ_{des}), a reference linear model with 2-DOF is adopted to estimate the lateral and yaw dynamic response as shown in Fig. 5. Tire lateral forces are calculated using linearized model by assuming constant cornering stiffness $C_{\alpha f}, C_{\alpha r}$ and slip angles α_f, α_r for front and rear tires.

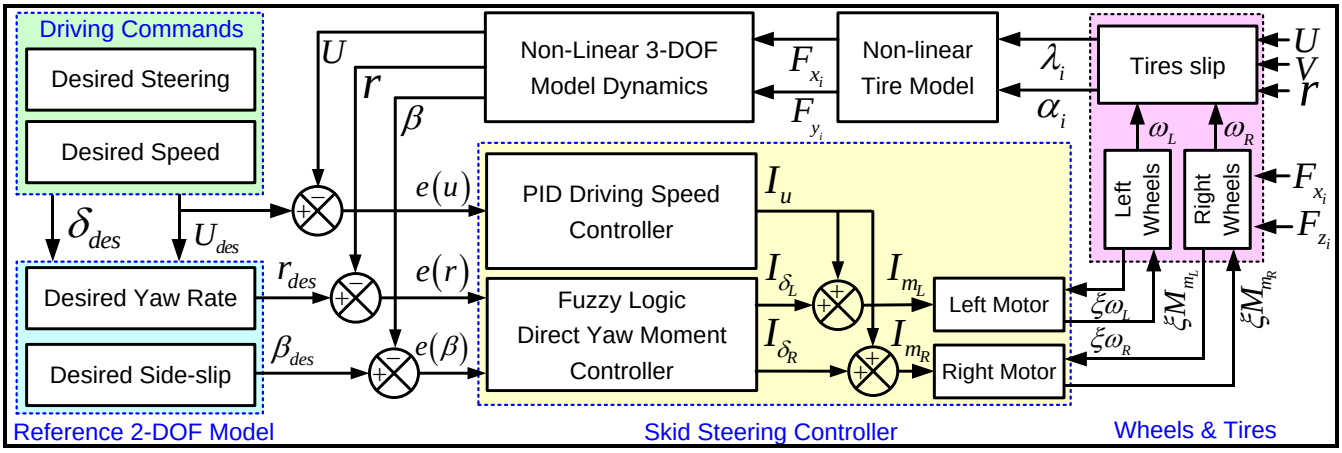

Fig. 4: General structure of the proposed skid steering control system

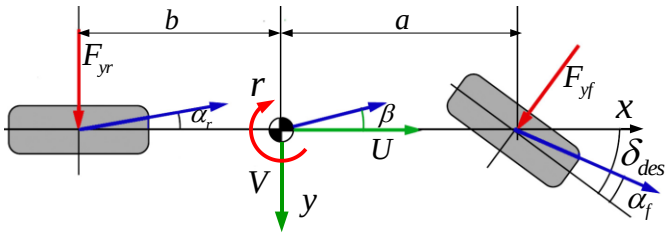

Fig. 5: Two-degrees of freedom bicycle vehicle model

The governing equations of motion of the 2-DOF bicycle vehicle model can be written in a matrix form as follows:

$$\begin{bmatrix} m & 0 \\ 0 & I_{zz} \end{bmatrix}\begin{bmatrix} \dot{V} \\ \dot{r} \end{bmatrix} = \begin{bmatrix} -\dfrac{C_{\alpha f}+C_{\alpha r}}{U} & \dfrac{-a\cdot C_{\alpha f}+b\cdot C_{\alpha r}}{U} \\ \dfrac{-a\cdot C_{\alpha f}+b\cdot C_{\alpha r}}{U} & -\dfrac{a^2\cdot C_{\alpha f}+b^2 C_{\alpha r}}{U} \end{bmatrix}\begin{bmatrix} V \\ r \end{bmatrix} + \begin{bmatrix} C_{\alpha f} \\ a\cdot C_{\alpha f} \end{bmatrix}\delta_{des} \quad (11)$$

The reference model estimates the steady-state desired yaw rate (r_{des}) and desired sideslip angle (β_{des}) relative to the change of the desired or virtual steering angle (δ_{des}) and vehicle forward velocity (U) as follows [14]:

$$r_{des} = \frac{U\cdot\delta_{des}}{L+\underbrace{\left(\dfrac{m\left(bc_{\alpha r}-ac_{\alpha f}\right)}{2c_{\alpha f}c_{\alpha r}L}\right)}_{understeer\ coefficient\ /\ g}U^2} \quad (12)$$

$$\beta_{des} = \frac{b-\left(\dfrac{ma}{2c_{\alpha r}L}\right)U^2}{L+\underbrace{\left(\dfrac{m\left(bc_{\alpha r}-ac_{\alpha f}\right)}{2c_{\alpha f}c_{\alpha r}L}\right)}_{understeer\ coefficient\ /\ g}U^2}\cdot\delta_{des} \quad (13)$$

3.2 PID Driving Speed Control

Referring to (12) and (13), both the desired yaw rate and side slip angle are dependent on the driving speed. Therefore, to ensure accurate control of the UGV x-y trajectory, the speed should be accurately controlled. For this purpose, a PID controller is employed to minimize the error in driving speed $\left(e(U)=U_{des}-U\right)$ as follows:

$$I_u = K_p e(U)+K_i\int e(U)\,dt+K_d\frac{de(U)}{dt} \quad (14)$$

Where (I_u) is the controlled current supplied to each motor to maintain the driving speed at its desired value. (K_p, K_i, K_d) are the gains of the PID controller which are obtained based on Ziegler–Nichols tuning method [15].

3.3 Fuzzy Logic Direct Yaw-moment Controller (DYC)

Direct yaw-moment control (DYC) is widely applied for modern vehicles in order to improve its directional stability during critical maneuvers. Generally, this method is introduced to generate an external (or counter) yaw moment by altering the individual wheels torque balance [16].

For internal combustion engine driven-vehicles, DYC is achieved by individually (differentially) actuating the wheel braking torque which in turn is limited by the overall braking system characteristics and has a negative consequence on reducing the vehicle speed. On the other hand, for electric motors driven-vehicles, DYC is effectively implemented with offering the advantages of smoothly and continuously vectoring the magnitude and direction of the driving torque among wheels.

In this paper, a fuzzy logic controller is employed to calculate the electric current $(I_{\delta L}, I_{\delta R})$ and therefore electric motor torques (M_{m_L}, M_{m_R}) necessary to generate a direct yaw moment (M_{DYC}) to control the UGV trajectory as follows:

$$M_{DYC} = \frac{c\xi\left(M_{m_L}-M_{m_R}\right)}{r_d} \quad (15)$$

The developed controller is continuously monitoring the actual yaw rate (r) and side slip angle (β) of the UGV body and therefore calculates the instantaneous yaw rate error $e(r)$ and side slip angle error $e(\beta)$ as follows:

$$\left.\begin{aligned} &Yaw\ Rate\ Error: && e(r)=r_{des}-r \\ &Side\ Slip\ Angle\ Error: && e(\beta)=\beta_{des}-\beta \end{aligned}\right\} \quad (16)$$

It should be noted that, the total controlled current supplied to each motor (I_{m_L}, I_{m_R}) is calculated to achieve the desired vehicle driving speed and the steering angle as follows:

$$\left.\begin{aligned} I_{m_L} &= I_u + I_{\delta_L} \\ I_{m_R} &= I_u - I_{\delta_R} \\ I_{\delta_L} &= I_{\delta_R} = I_\delta \end{aligned}\right\} \quad (17)$$

Assuming that the UGV body is symmetrical about its longitudinal x-axis and using identical electric motors for left and right sides, the controlled current for each motor is reasonably assumed to be equal as given in (17).

Fuzzy logic control is a knowledge-based control method which is based on empirical experience for controlling

systems. It is widely applied because of the convenience it offers in the control of non-linear dynamic systems.

For each input of the FL controller, five membership functions are selected as shown in Fig. 6 (a - b) including two trapezoidal and three triangle membership functions with the following variables: high negative (HN), low negative (LN), zero (ZO), low positive (LP), high positive (HP).

The controlled parameters of the electric current for both left and right motors $(I_{\delta L}, I_{\delta R})$ are obtained based on the calculated yaw rate and side-slip angles errors with a scaling factor. For this purpose, eleven membership functions are considered including two trapezoidal and nine triangle membership functions as illustrated in Fig. 6 (c). These variables are; N5, N4, N3, N2, N1, ZO, P1, P2, P3, P4, and P5. Furthermore, the rule base of the direct yaw-moment controller using fuzzy logic control is given in Table. 1.

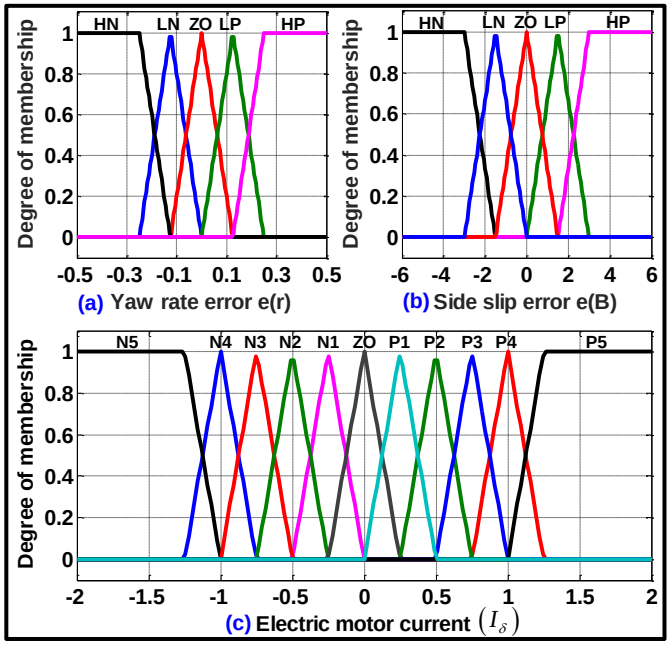

Fig. 6: Membership functions of Direct Yaw-moment Controller

Table 1. Rule base for DYC Fuzzy Logic Controller

		Side Slip Angle Error				
		HN	**LN**	**ZO**	**LP**	**HP**
Yaw Rate Error	**HN**	N1	N1	ZO	P1	P1
	LN	N2	N2	ZO	P2	P2
	ZO	N3	N3	ZO	P3	P3
	LP	N4	N4	ZO	P4	P4
	HP	N5	N5	ZO	P5	P5

4. Results and discussions

The non-linear second order equations of motion of the derived 5-DOF model are successfully solved and simulated in MATLAB/Simulink environment. Additionally, *Fuzzy Logic Toolbox* is used to implement fuzzy logic rules of the direct yaw moment control. In this section, different simulations are presented to check the fidelity of the proposed controller.

4.1 Model Verification

In order to ensure accurate results from the proposed model, the output is compared to that of a well-published paper [17]. For this purpose, the presented model is modified to include Ackermann steering system and considered similar input data during the same cornering conditions of single lane change maneuver at high speed of 20 m/s.

From the comparison of Figs. 7 and 8, it can be concluded that, the vehicle trajectory, yaw rate and lateral acceleration of the vehicle body for both models are found to be in good agreement which reflects sufficient accuracy of the proposed model.

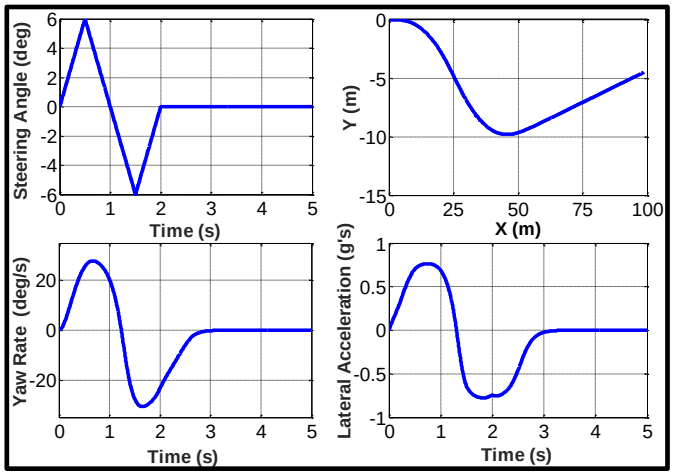

Fig. 7: Results of the derived 5-DOF model with Ackermann steering

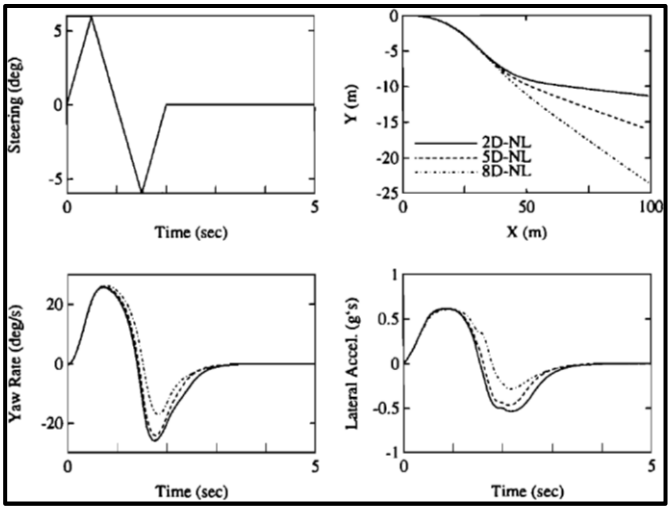

Fig. 8: Time response of a published work with Ackermann steering [16]

4.2 Ackermann versus Skid Steering Control System

The derived 5-DOF model is employed to compare the response of body dynamics with Ackermann steering system and that of fuzzy logic controlled skid-steered UGV as shown in Figs. 10 to 12.

A single lane change maneuver is considered by applying a single sine waveform of an amplitude 148° at the steering wheel within eight seconds full period as shown in Fig. 9. It should be noted that, for skid-steered vehicle, the wheels are not steered, therefore the desired steering angle is virtually employed to calculate the reference yaw rate and side slip angle. Consequently, the skid steering controller calculates the direct yaw moment and the electric current necessary to regulate the driving torque for each motor independently.

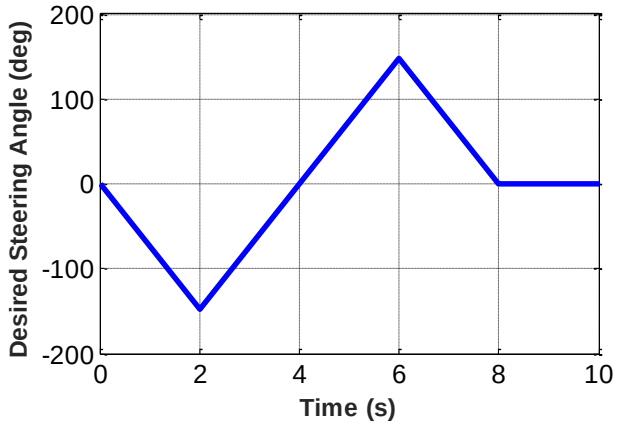

Fig. 9: Desired steering angle – single lane change maneuver

For the purpose of accurate control of the UGV trajectory, the vehicle driving speed should be controlled as described in section 3. As illustrated in Fig. 10, the driving speed is successfully controlled at constant relatively higher value of 20 m/s (72 km/h) without a noticeable difference between Ackermann and skid steering systems. On the other hand, the time-response of the lateral velocity shows little delay and peak-reduction for the vehicle with Ackerman steering compared to that form skid steering system, see Fig. 11.

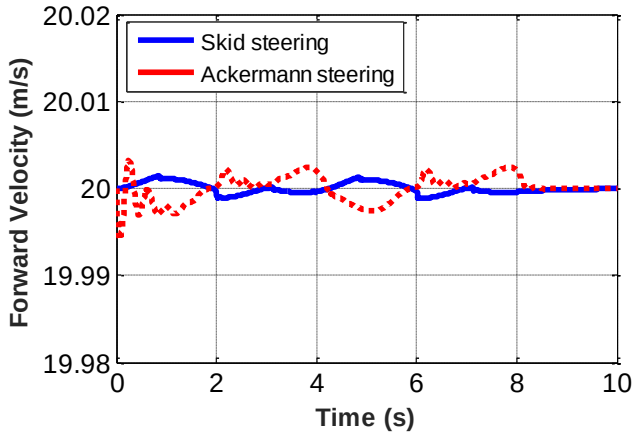

Fig. 10: Controlled vehicle driving (forward) velocity

The cornering response of the UGV body in terms of yaw rate and side slip angle is illustrated in Figs. 12 and 13 respectively with fairly comparison between the reference control signal, Ackermann and skid steering systems. While all the output results follow the same input sinusoidal pattern of lane change maneuver, it is obvious that, for the proposed skid-steered controller, the UGV cornering response follows the desired profile more precisely than that of the conventional Ackermann system. Additionally, applying the direct yaw moment controller enables the UGV to reaches its desired response in shorter time than that of Ackermann steering.

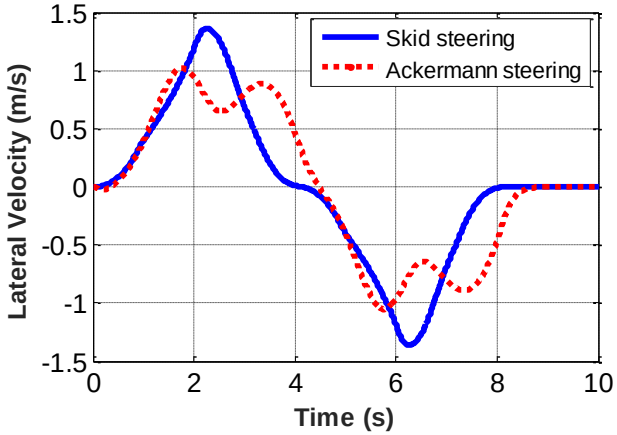

Fig. 11: Vehicle later velocity – single lane change, 20 m/s

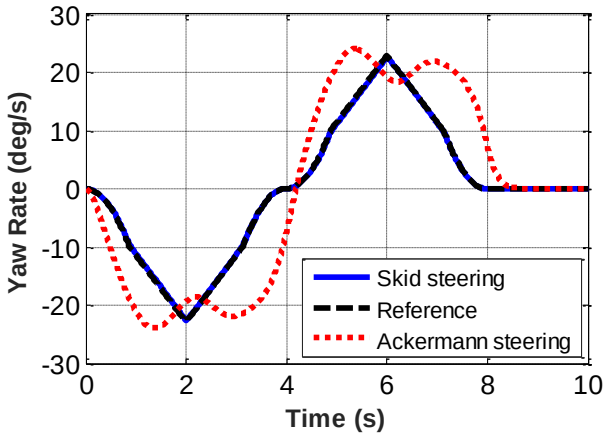

Fig. 12: Vehicle body yaw rate – single lane change, 20 m/s

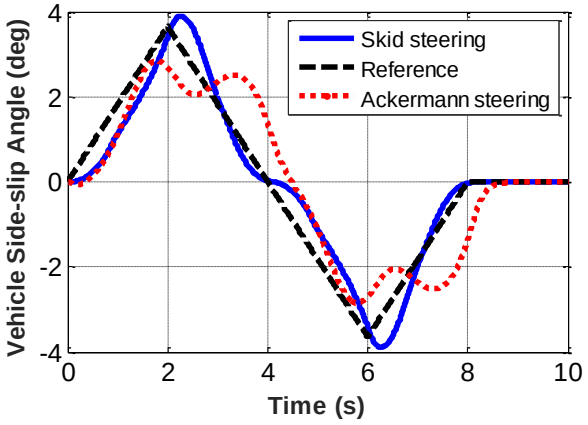

Fig. 13: Vehicle side slip angle – single lane change, 20 m/s

From the observation of the UGV response with skid-steered controller, both the reduction in lateral velocity and increase of controlled yaw rate enable the UGV to perform lane change maneuver with less offset in the lateral direction (30 m) compared to that provided by Ackermann steering system as shown in Fig. 14.

On the other hand, for the same simulation time, longer distance is achieved by the vehicle with skid-steered system with 23 m more than that of the Ackermann steering system. This result emphasizes the outcome of implementing an accurate control of independent electric motors to minimize the turning curvature of skid-steered UGVs.

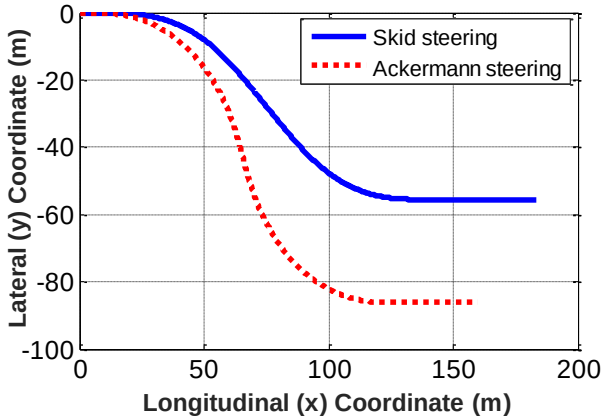

Fig. 14: Vehicle body trajectory – single lane change, 20 m/s

4.3 Control Action of the Proposed Skid Steering System

The control action of the proposed skid steering controller is examined by illustrating the dependency of the output wheels driving torques, wheels angular speeds and the input desired steering wheel angel as shown in Figs. 15 and 16 respectively.

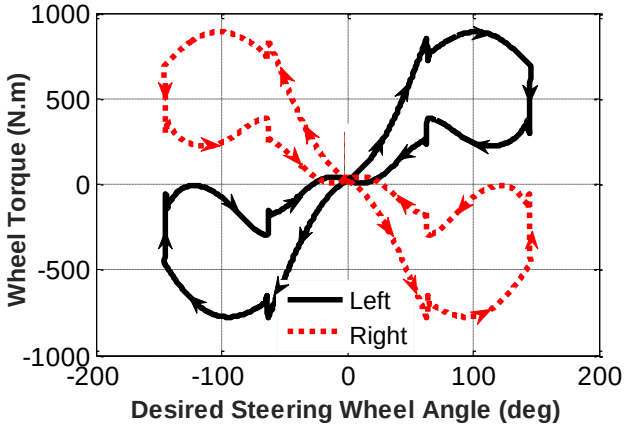

Fig. 15: Wheels driving torque – single lane change, 20 m/s

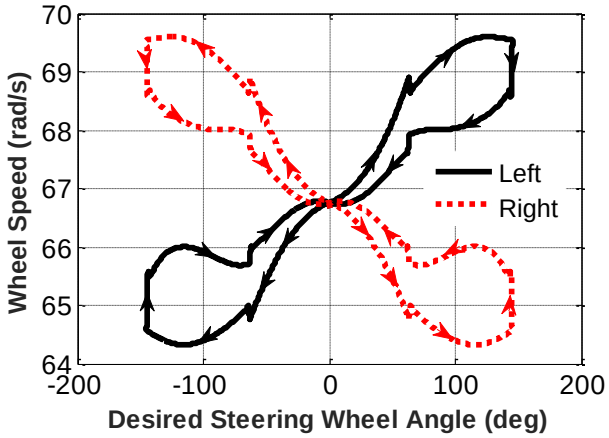

Fig. 16: Wheels angular speed – single lane change, 20 m/s

The simulation is carried out during the same cornering conditions of single lane change maneuver shown in Fig. 8 and at a constant forward speed of 20 m/s. It is clear that, as the desired steering angle increases, the differential driving torque and consequently differential speed between left and right wheels increases in a similar sinusoidal shape which enables the vehicle to perform the desired steering pattern.

As a result of controlling the wheels driving torques and therefore wheels angular speeds, the tire forces in longitudinal direction and their associated longitudinal slips are generated in similar pattern as shown in Figs. 17 and 18 respectively.

It should be noted that, for the same side, there is a little difference between the front and rear longitudinal forces which is referred to the variation in vertical weight imposed upon each wheel. Although the vehicle driving speed is kept constant (very small forward acceleration), higher values of both tire driving torques and longitudinal forces are developed which reflects an adhered criteria for wheeled vehicles with skid steering system to perform the desired cornering of the vehicle.

Equations (8) and (9), can be used to justify the positive and negative signs of the tire longitudinal slip and therefore tire longitudinal forces for the outward and inward wheels respectively during turning.

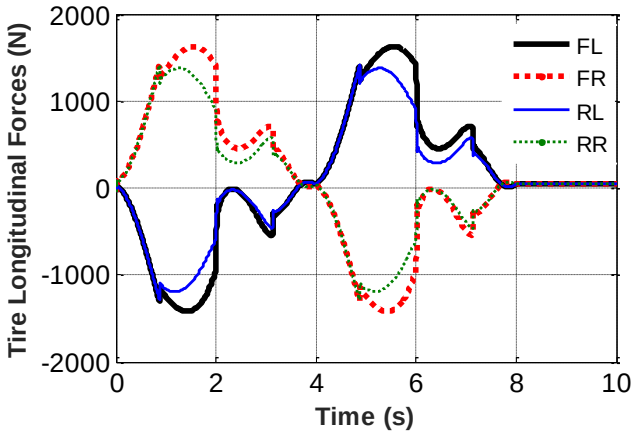

Fig. 17: Tire longitudinal forces – single lane change, 20 m/s

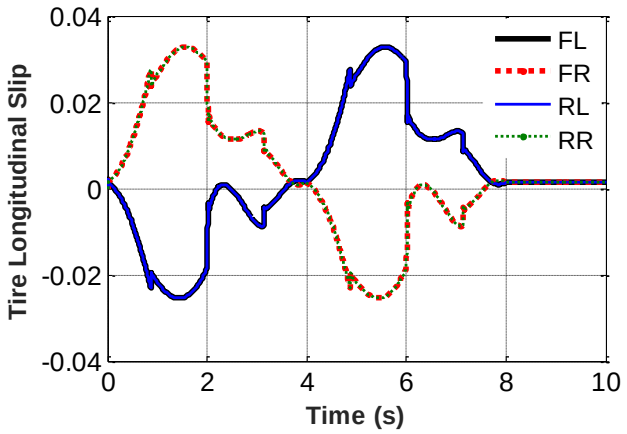

Fig. 18: Tire longitudinal slip – single lane change, 20 m/s

On the other hand, the tire lateral forces and their associated lateral slips follow the same pattern of the desired steering angle with small difference between front and rear tires as shown in Figs. 19 and 20 respectively. Since the roll dynamics is not considered in this paper, there is no significant difference between both left and right tires lateral forces and slips.

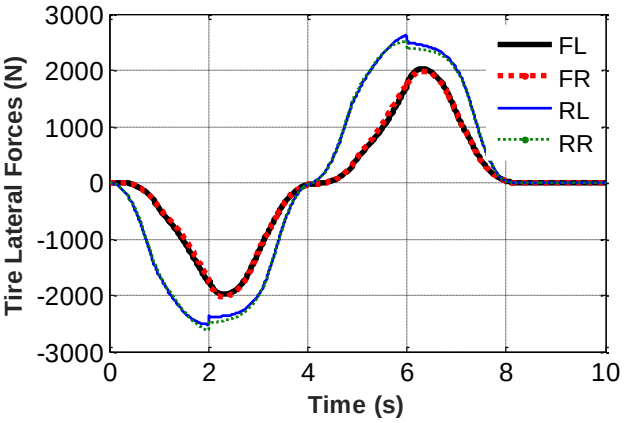

Fig. 19: Tire lateral forces – single lane change, 20 m/s

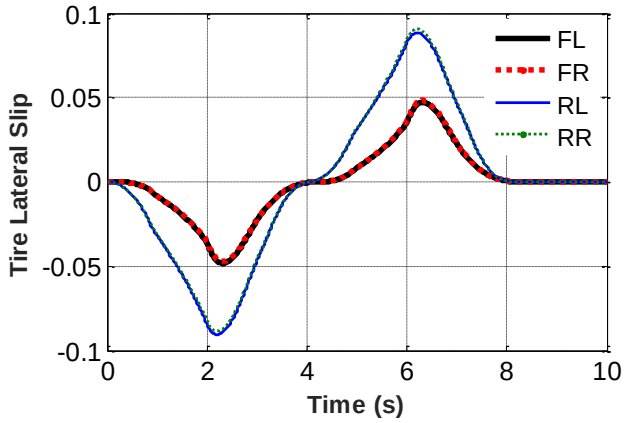

Fig. 20: Tire lateral slip – single lane change, 20 m/s

4.4 The Control Parameters of the UGV x-y Trajectory

Referring to (12), for fixed UGV design parameters and weight distribution, the desired yaw moment and therefore x-y trajectory depends up on both the driving forward speed and the desired steering profile.

To illustrate this effect, each parameter is changed separately by varying the amplitude of the desired steering angle as shown in Fig. 21 and by changing the vehicle driving speed as shown in Fig. 22. It should be mentioned that, the output torque from left and right electric motors is independently controlled to achieve the desired steering and driving speed as required. From the comparison of Figs. 21 and 22, it can be concluded that, for fixed driving speed, the x-y trajectory of the UGV can be easily controlled in a wider range.

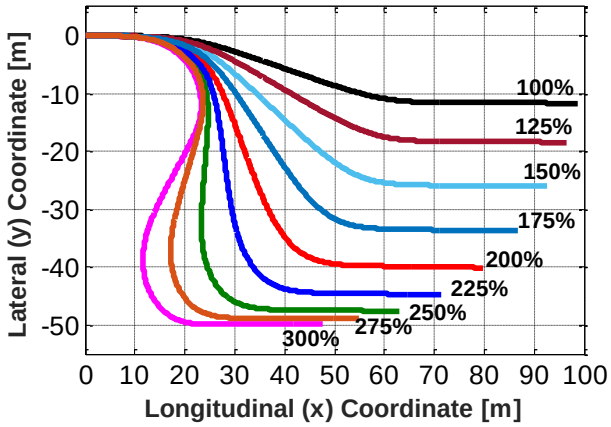

Fig. 21: Trajectory control by desired steering angle at 20 m/s

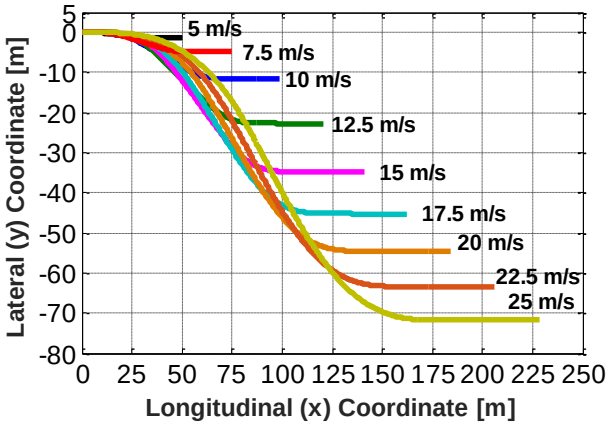

Fig. 22: Trajectory control by vehicle speed – same steering profile

4.5 x-y Trajectory for Different Desired Cornering Maneuvers

To check the potential of the proposed skid steering control system to perform different cornering scenarios, additional two steering-profiles are employed.

For each steering profile, the results of *x-y* trajectory for different conditions are plotted as shown in Figs. 23 and 24 respectively. In Fig. 23, a ramp steer maneuver is considered in which the desired steering angle is linearly and slowly increased with time.

The results are shown during different constant driving speeds; 10, 15 and 20 m/s. As previous concluded, increasing UGV driving speed results in higher desired yaw rate and therefore larger UGV trajectory.

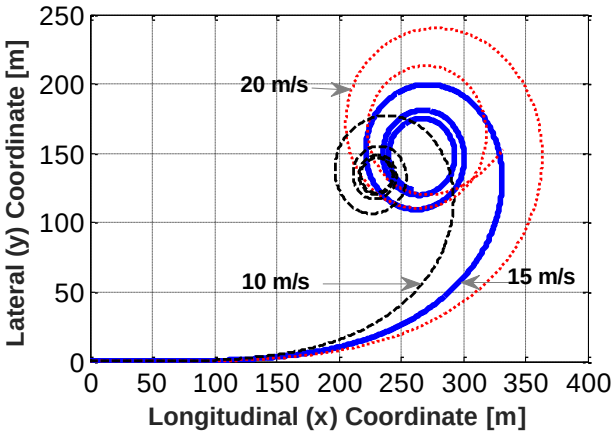

Fig. 23: UGV x-y trajectory during ramp steer maneuver and different driving speed (10, 15 and 20 m/s)

In Fig. 24, a J-turn or constant radius steer maneuver is considered such that a constant steering angle is used to generate constant yaw rate for the skid-steered controller to perform the desired turn. While the driving speed is controlled at 10 m/s, different constant values of steering angles are used. It should be mentioned that, for skid steering systems, the minimum turning radius is depending up on the power and torque applied by each motor.

On the other hand, the maximum applied torque is limited by the possible tire-road adhesion. Further application of the driving torque results in more wheel slip and failure to perform the desired steering angle. The obtained results of UGV during different cornering maneuvers reflect the fidelity of the propped skid steering control system.

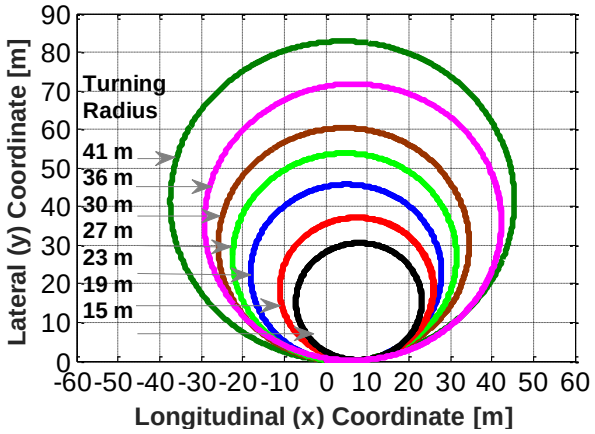

Fig. 24: UGV x-y trajectory during J-Turn maneuver and constant driving speed (10 m/s) for different turning radii (15, 19, 23, 27, 30. 36 and 41 m)

4.6 Power of the Electric Motors

An important factor for skid steering systems, is the choice of the electric motors in terms of power and torque speed characteristics. Generally, electric motors power depends on vehicle weight, desired driving speed and cornering scenario. When the vehicle weight increases, tires vertical force increase as well which requires higher motors power to generate sufficient tire longitudinal and lateral forces necessary to build up the required yaw moment to turn the vehicle appropriately.

The effect of driving speed on electric motors power and torque during single lane change maneuver are shown in Figs. 25 and 26 considering two driving speeds 10 and 20 m/s. it is obvious that, increasing the driving speed increases both the value and variation of power and torque during the turn. This is obviously true, since the desired yaw rate and side slip angle are speed dependent as given in (12) and (13) respectively.

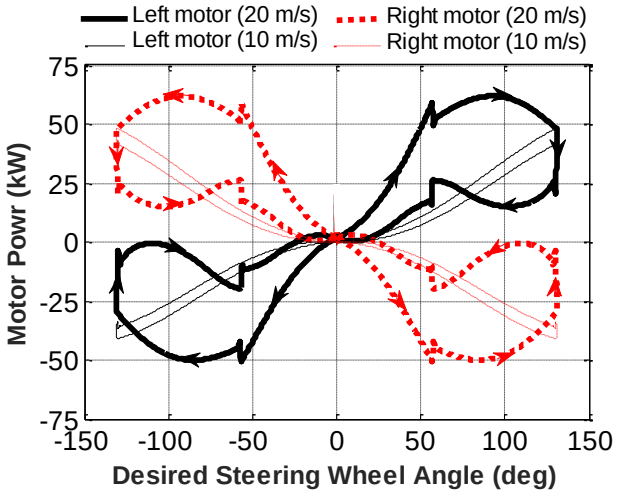

Fig. 25: Effect of driving speed on the demand power- same steering profile

The effect of steering on electric motors power is shown in Fig. 27 considering different amplitudes 50%, 72%, 125% and 150% of the bassline value of single lane change maneuver at constant driving speeds 10 m/s. it is obvious that, increasing the amplitudes of the steering angle increases the required motor power to perform the desired maneuver. This is particularly true because during tight cornering maneuvers, higher longitudinal and lateral tire forces are required which in turn increase the required power of the electric motors.

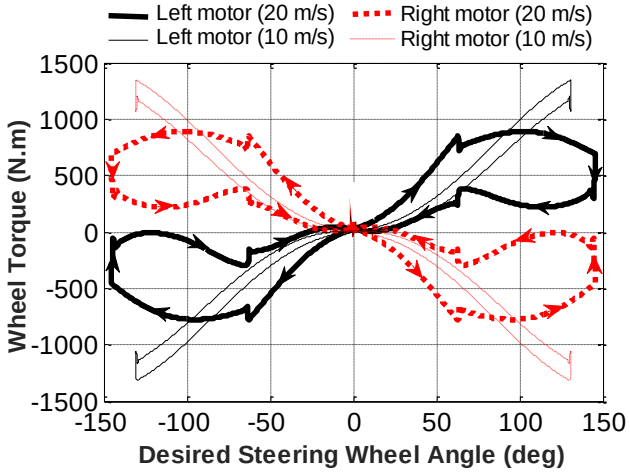

Fig. 26: Effect of driving speed on the demand torque - same steering profile

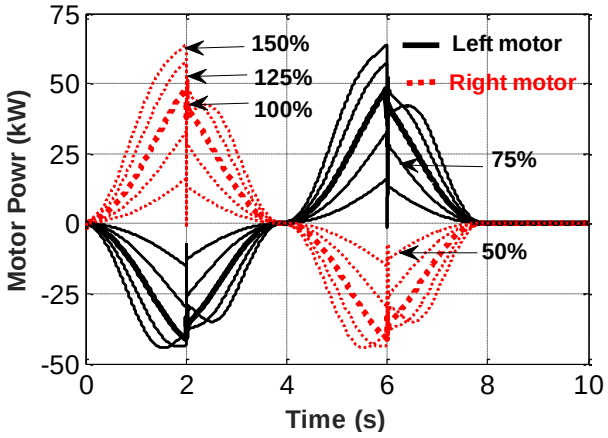

Fig. 27: Effect of the steering - same driving speed (10 m/s)

5. Conclusions

In this paper, a non-linear skid steering control system for unmanned ground vehicles is introduced. Based on direct yaw moment method, a fuzzy logic controller is proposed to individually control the electric motor and therefore output wheel torque for a given UGV to follow desired driving speed as well as steering profile. The UGV dynamics is represented with five degrees of freedom and a non-linear tire model is used to calculate the tire forces in longitudinal and lateral directions.

A fairly comparison of the vehicle dynamics with conventional Ackermann and the proposed skid-steered systems is carried out. The results show the benefits of the presented skid steering system to accurately follow both the desired yaw rate and side-slip angle. In addition, the cornering maneuver is performed with shorter lateral offset and longer forward distance. On the other hand, it has been shown that, for skid steering system, higher driving wheel torque and traction forces are required to perform the desired cornering maneuver.

The proposed control system is used to illustrate the x-y trajectory during different maneuvers such as ramp and-steer and constant radius tests. In addition, different factors affecting selection of the motor power are investigated.

The main contribution of this paper is to develop more accurate and realistic skid steer control system suitable for UGVs with relatively higher weight and driving speeds during transient and abrupt change maneuvers. Accordingly, both vehicle body dynamics and tire forces are properly incorporated. This is particularly true since the majority of published relevant work is mostly devoted to wheeled mobile robots with simplified kinematical models or linearized tire formulas and driven at low speed.

Nomenclature

A_f	Vehicle frontal area
C_d	Coefficient of air resistance
C_α	Tire cornering stiffness
$F_{x_i}, F_{y_i}, F_{z_i}$	Tire forces in longitudinal, lateral and vertical directions
I_u	Motor controlled current
I_{m_L}, I_{m_R}	Left and right electric motor currents
I_{zz}	Sprung mass moment of inertia about z-axis
I_{δ_L}, I_{δ_R}	controlled current for left and right motors
J_{eq}	Motor equivalent mass moment of inertia
L	Vehicle wheelbase
M_{m_L}, M_{m_R}	Left and right electric motor torques
M_{DYC}	Direct yaw moment
U, V	Vehicle velocities in x and y directions
a, b	Sprung mass CG from front and rear axles
a_x, a_y	forward and lateral accelerations
c	Half wheel-track
h	Sprung mass CG height
m	Vehicle sprung mass
r, r_{des}	Sprung mass yaw rate and desired yaw rate
r_d	Tire dynamic radius
t_p	Tire pneumatic trail
u_{x_i}, v_{y_i}	Wheel linear velocities in x and y directions
α_i	Tire slip angles
β, β_{des}	side slip angle and desired side slip angles
δ, δ_{des}	Steering angle and desired steering angles
λ_i	Tire longitudinal slip ratios
ξ	Mechanical transmission ratio
ρ	Air density
ω_i	Wheel angular speeds

Acknowledgement

The author wishes to express his gratitude to the Egyptian Armed Forces for the financial support extended to this research project.

References

[1] Villiam R. Meldrum, Francis B. Hoogterp and Alexander R. Kovnat 'Modeling and simulation of a differential torque steered wheeled vehicle', Technical Report 13777, U.S. Army Tank-Automotive Research, Development, and Engineering Center, Detroit Arsenal, Warren, Michigan 48397-5000, July 1999.

[2] Maclaurin, B. 'Comparing the steering performances of skid-steered and Ackermann-steered vehicles', *Proceeding of the Institution of Mechanical Engineers, Part D: Journal of Automobile Engineering*, 222, 5, 739-756, 2008.

[3] W. Li, T.E.C. Potter and R.P. Jones, 'Steering of 4WD vehicles with independent wheel torque control', *Vehicle System Dynamics* (Supplement), 28, pp.205-218, 1998.

[4] Krzysztof Kozlowski and Dariusz Pazderski 'Modelling and control of a 4-wheel skid steering mobile robot', *International Journal of Applied Mathematics and Computer science*, Vol. 14, No.4, pp. 477-496, 2004.

[5] Gao Shuang, Norbert C. Cheung, K.W. Eric Cheng , Dong Lei and Liao Xiaozhong 'Skid steering in 4WD EV', Power Electronics and Drive Systems, 2007, 7th International Conference, IEEE, pp. 1548-1553, 2007.

[6] Zhang Yu, Hu Jibin, Li Xueyuan, Lyu Shupeng and Guo Jing 'A linear lateral dynamic model of skid steered wheeled vehicle', Intelligent Vehicles Symposium (IV), IEEE, pp.964 - 969, 1931-0587, 2013.

[7] Yu Zhang, Jibin Hu and Xueyuan Li 'Steady-state characteristics of skid steering for wheeled vehicles', *Proceedings of the Institution of Mechanical Engineers, Part D: Journal of Automobile Engineering*, Vol. 228(9) 1095–1104, 2014.

[8] David Milner, Jarrett Goodell, Wilford Smith, Mike Pozolo and Jason Ueda 'Modeling and simulation of an autonomous hybrid electric military vehicle', Proceedings of the EVS24 International Battery, Hybrid and Fuel Cell Electric Vehicle Symposium, Stavanger, Norway, May 137-16, 2009.

[9] Juyong Kang, Wongun Kim, Kyongsu Yi, Soungyong Jung and Jongseok Lee 'Skid steering based driving control of a robotic vehicle with six in-wheel drives', *SAE Int. J. Passeng. Cars – Mech. Syst*., Volume 3, Issue 1, 2010-01-0087, 2010.

[10] Jaewon Nah, Seungjae Yun, Kyongsu Yi, Wongun Kim and Jongbae Kim 'Driving control architecture for six-in-wheel-driving and skid-steered series hybrid vehicles', Proceedings of the EVS27 International Battery, Hybrid and Fuel Cell Electric Vehicle Symposium, Barcelona, Spain, November 17-20, 2013.

[11] L. Tong, L. Wei, W. BeiLe and L. Yu Qian 'Dynamic control algorithm design of the 6 wheel-drive all-terrain robotic skid-steered vehicles', Guidance, Navigation and Control Conference (CGNCC), 2014 IEEE Chinese, Yantai, pp. 2713-2718, 2014.

[12] Changjun Kim, Ali Mian Ashfaq, Sangho Kim, Sunghoon Back, Youngsoo Kim, Soonwoong Hwang, Jaeho Jang, and Changsoo Han , 'Motion Control of a 6WD/6WS Wheeled Platform with In-wheel Motors to Improve Its Maneuverability', *International Journal of Control, Automation, and Systems*, 13(2):434-442, 2015.

[13] H.B. Pacejka and I.J.M. Besselink, 'Magic Formula Tyre Model with Transient Properties', in F. Bohm and H.-P. Willumeit, Eds., Proc. 2nd Int. Colloquium on Tyre Models for Vehicle Dynamic Analysis, Berlin. Lisse, The Netherlands: Swets & Zeitlinger, 1997.

[14] R. Rajamani, '*Vehicle Dynamics and Control*', Springer Science & Business Media, 2011.

[15] K.Ogata, '*Modern Control Engineering*', 5th edition, Prentice Hall, 2010.

[16] Simanta Ghosh, Anindya Deb, Manoj Mahala, Morteza Tanbakuchi and Matthew Makowski, 'Active Yaw Control of a Vehicle using a Fuzzy Logic Algorithm', SAE paper no. 2012-01-0229, 2012.

[17] Smith, D.E. and Starkey, J.M., 'Effects of Model Complexity on the Performance of Automated Vehicle Steering Controllers: Model Development, Validation and Comparison', *Vehicle System Dynamics*, Volume 24(1995), pp. 163-181, 1995.